

# Soft X-rays from polar caps of the millisecond pulsar J0437–4715

V. E. Zavlin<sup>1</sup>, \* and G. G. Pavlov<sup>2,1</sup>

<sup>1</sup> Max-Planck-Institut für Extraterrestrische Physik, Giessenbachstrasse, D-85740 Garching, Germany

<sup>2</sup> Pennsylvania State University, 525 Davey Lab, University Park, PA 16802, USA

November 10, 2021

**Abstract.** We show that the soft X-ray spectra and light curves observed with the *ROSAT* and *EUVE* from the closest known millisecond pulsar J0437–4715 can be interpreted as thermal radiation from two hot polar caps whose emitting layers (atmospheres) are comprised of hydrogen. The simplest model yields a uniform temperature of  $(0.8 - 0.9) \times 10^6$  K within a cap radius of 0.7–0.9 km. The spectral fits indicate that the temperature may be nonuniformly distributed along the cap surface. The distribution can be approximated by a central core heated up to  $(1 - 2) \times 10^6$  K within a radius of 0.2–0.4 km, surrounded by a colder rim with temperatures  $(3 - 5) \times 10^5$  K extending out to 2–6 km. The polar cap interpretation implies low column densities,  $(1 - 3) \times 10^{19}$  cm<sup>-2</sup>, and a high degree of ionization, > 20%, of the interstellar hydrogen towards the pulsar. The inferred bolometric luminosity of the polar caps,  $(1.0 - 1.6) \times 10^{30}$  erg s<sup>-1</sup>, is in excellent agreement with the predictions of the slot-gap model of radio pulsars developed by Arons and his coworkers. Similar polar cap radiation should be emitted by other millisecond pulsars, although in some of them (e. g., PSR B1821–24) the soft X-ray flux is dominated by the nonthermal radiation from pulsar magnetospheres.

**Key words:** stars: neutron – X-ray: stars – pulsars: individual: PSR J0437–4715

## 1. Introduction

The bright 5.75 ms pulsar J0437–4715 was discovered by Johnston et al. (1993) during the Parkes survey for millisecond pulsars. The pulsar is in a 5.74 d binary orbit with a cool ( $T_{\text{color}} \simeq 4000$  K), low-mass ( $\sim 0.2M_{\odot}$ ) white dwarf companion and is surrounded by a bow-shock nebula (Becker et al. 1993; Bailyn 1993; Bell, Bailes & Bessel 1993; Danziger, Baade & Della Valle 1993; Bell

et al. 1995). It is an old object, with a characteristic age  $\tau = P/2\dot{P} \simeq 5 \times 10^9$  yr, low magnetic field  $B \sim 3 \times 10^8$  G, and rotational energy loss  $\dot{E} = 4 \times 10^{33}$  erg s<sup>-1</sup>. The observed dispersion measure of 2.65 pc cm<sup>-3</sup> implies a distance  $d \simeq 100 - 180$  pc, making this the closest known millisecond pulsar. Sandhu et al. (1997) reported the distance  $d = 178 \pm 26$  pc, from parallax measurements. The pulsar shows significant radio emission over at least 80% of the pulse period, with a complicated mean pulse shape varying with radio frequency. Variation of the linear polarization position angle within the mean pulse interpreted in terms of the rotating vector model (Radhakrishnan & Cooke 1969) yields the angle between the observer’s line of sight and the rotation axis,  $\zeta \simeq 40^\circ$ , and the angle between the magnetic and rotation axes,  $\alpha \simeq 35^\circ$  (Manchester & Johnston 1995).

*ROSAT* observations of PSR J0437–4715 with the Position Sensitive Proportional Counter (PSPC) have revealed (Becker & Trümper 1993; hereafter BT93) that this is also a bright (count rate =  $0.204 \pm 0.006$  s<sup>-1</sup>) soft X-ray pulsar with a single broad pulse and a pulsed fraction  $f_p = 33 \pm 3\%$  in the PSPC energy range 0.1–2.4 keV. BT93 found that the pulsed fraction varies with photon energy  $E$  and peaks in the range 0.6–1.1 keV, reaching  $53 \pm 6\%$ . Although the pulsar spectrum can be fitted with a single power law, indicative of a non-thermal origin of the soft X-ray radiation, the energy dependence of the pulsed fraction in the narrow energy range makes this interpretation hardly plausible. BT93 showed also that a single blackbody model does not fit the PSPC spectrum leaving a residual hard excess above 0.4 keV. They suggested that the spectrum can consist of two components: a power law, representing magnetospheric or nebular emission, and a blackbody component of the temperature  $T \sim 1.7 \times 10^6$  K emitted from an area of  $\sim 0.08 d_{180}^2$  km<sup>2</sup> ( $d_{180} = d/180$  pc); this thermal component was suggested by BT93 to be radiated from a hot spot on the neutron star (NS) surface.

\* e-mail: zavlin@mpe-garching.mpg.de

PSR J0437–4715 was also detected with the *EUVE* Deep Survey Instrument (DSI) in the Lexan band filter ( $E \simeq 0.05 - 0.2$  keV) by Edelman, Foster & Bowyer (1995) and Halpern, Martin & Marshall (1996; hereafter HMM96). According to Edelman et al. (1995), the DSI count rate of the source is  $0.0143 \pm 0.0008$  s $^{-1}$ , whereas HMM96 report the count rate of  $0.00973 \pm 0.00017$  s $^{-1}$  obtained with a much longer exposure (496 ks vs. 72 ks). Edelman et al. (1995) ruled out the single power-law spectral model based on the improbably high hydrogen column density,  $n_H = 2.5 \times 10^{20}$  cm $^{-2}$ , required by this model. They claimed that both the *ROSAT* flux below 0.4 keV and the *EUVE* flux could arise from an isothermal blackbody with a temperature  $\sim 5.7 \times 10^5$  K, an emitting area of  $\sim 3$  km $^2$ , and an absorbing column of  $n_H = 5 \times 10^{19}$  cm $^{-2}$ . On the other hand, HMM96 concluded that the combined analysis of the *ROSAT* spectrum and *EUVE* flux is consistent with a single power-law spectrum of photon index  $\gamma = 2.2 - 2.5$  and intervening column density  $n_H = (5 - 8) \times 10^{19}$  cm $^{-2}$ . Alternatively, the combined data can be interpreted as comprised of two components, e. g., a power law and a blackbody component emitted from a hot polar cap of radius 50–600 m and temperature  $(1.0 - 3.3) \times 10^6$  K. HMM96 observed the pulsar in the high time resolution mode, which enabled them to obtain the light curve and to measure the pulsed fraction  $f_p = 27 \pm 5\%$  in the *EUVE* DSI spectral range.

Thus, although very important data have been collected and analyzed, the true nature of the soft X-ray radiation from PSR J0437–4715 remains elusive. The only firmly established facts are that the radiation is pulsed (pulsed fraction apparently depends on energy), and the spectrum cannot be fitted with a single blackbody model. The main question is whether the radiation is of a non-thermal (magnetospheric? nebular?) origin or at least a fraction of it can be interpreted as thermal (or thermal-like) radiation from some heated regions (polar caps?) on the NS surface.

Virtually all the (different) models of radio pulsars (e. g., Cheng & Ruderman 1980; Arons 1981; Michel 1991; Beskin, Gurevich & Istomin 1993) predict these objects to have *polar caps* (PCs) around the NS magnetic poles heated up to X-ray temperatures by relativistic particles and gamma-quanta impinging onto the pole regions from the acceleration zones. A conventional assumption about the PC radius is that it is close to the radius within which open magnetic field lines originate from the NS surface. For PSR J0437–4715, it gives  $R_{pc} = 1.9 (R_{NS}/10 \text{ km})^{3/2} (P/5.75 \text{ ms})^{-1/2}$  km. Expected PC temperatures,  $T_{pc} \sim 5 \times 10^5 - 5 \times 10^6$  K, and luminosities,  $L_{pc} \sim 10^{28} - 10^{32}$  erg s $^{-1}$ , are much less certain, being strongly dependent on the specific pulsar model. Thus, one cannot firmly predict PC properties because of the lack of a well-established pulsar model — rather a theoretical model should be chosen based on X-ray observations of radio pulsars.

X-ray observations of other old pulsars (e. g., PSR B1929+10 – Yancopoulos, Hamilton & Helfand 1994; PSR B0950+08 – Manning & Willmore 1994) do show pulsed X-ray radiation which, in principle, could be the thermal PC radiation. However, the number of photons collected has been too small to make firm conclusions, and the opposite hypothesis, that this radiation is of a magnetospheric origin (Ögelman 1995; Becker & Trümper 1997 – hereafter BT97), cannot be excluded. In principle, one could also observe the PC radiation from younger pulsars and use these data to discriminate between different PC models. Indeed, there are some indications that hard components of the soft X-ray spectra of, e. g., PSR B0656+14 and PSR B1055–52 (Greiveldinger et al. 1996) may consist of two subcomponents, a power law and a thermal subcomponent corresponding to emission from PCs of temperatures  $T_{pc} \sim 1.5 \times 10^6$  K (for PSR B0656+14) and  $\sim 3.7 \times 10^6$  K (for PSR B1055–52). This interpretation, however, is not unique because it is difficult to separate the hard component from the soft one which is believed to originate from the (cooler) entire NS surface, and even more difficult to separate the two subcomponents of the hard spectral tail.

One cannot also exclude *a priori* that the nonthermal radiation from the pulsar magnetosphere or a pulsar-powered compact nebula contributes to, or even dominates, the observed soft X-ray flux of PSR J0437–4715. It is natural to assume that the spectrum of this radiation can be approximated by a power law in the relatively short *EUVE-ROSAT* range. One could also expect the magnetospheric (but not nebular) radiation to be pulsed with the radio pulsar period; the pulses should be, as a rule, narrower than those of the thermal PC radiation, and the shape of the light curve should not vary considerably with photon energy. Thus, if more data confirm the conclusion of BT93 that the pulsed fraction depends on  $E$ , the radiation of PSR J0437–4715 should either be thermal or consist of the thermal and nonthermal components. In the latter case, since the sources of the thermal and nonthermal radiation are expected to be spatially separated, it is natural to expect that pulsations of these two components should be phase-shifted due to the difference of travel times and aberration. For instance, if the nonthermal component is generated at a distance comparable to the light cylinder radius ( $R_{lc} \sim Pc/2\pi \sim 3 \times 10^7$  cm), the time delay leads to a phase shift of about 0.2 of the pulsar period. No energy-dependent phase shifts have been reported for this source, although it can be explained by the poor photon statistics in hard PSPC channels.

As in the case of thermal PC radiation, the current theoretical models of nonthermal high-energy pulsar emission (e. g., Sturmer, Dermer & Michel 1995; Romani 1996) are not enough elaborated to predict the intensity, spectrum and light curve for a given pulsar. There exist empirical formulae (Seward & Wang 1988; Ögelman 1995; BT97) which relate the (presumably nonthermal) X-ray luminosity to the pulsar parameters, e. g.,

to the period and magnetic field. For instance, Ögelman (1995) pointed out that the observed soft X-ray luminosities satisfy, for 7 pulsars, the following equation:  $L_x \simeq 6.6 \times 10^{26} (B_{12}/P^2)^{2.7} \text{ erg s}^{-1} \propto \dot{E}^{1.35}$ . BT97 fitted the luminosities of 26 pulsars observed in the *ROSAT* range with the dependence  $L_x \simeq 0.001\dot{E}$ . These pulsars represent a very wide range of spin-down luminosities ( $10^{33} - 10^{39} \text{ erg s}^{-1}$ ), ages ( $10^3 - 7 \times 10^9 \text{ yr}$ ), magnetic field strength ( $10^8 - 10^{13} \text{ G}$ ) and spin periods (1.6 – 530 ms). The inferred dependence indicates that for most pulsars the bulk of observed radiation is directly connected with pulsar mechanisms, i. e., with production and acceleration of relativistic particles which carry away the NS rotational energy. The fact that X-rays from some of these pulsars (e. g., Crab) are certainly nonthermal may allow one to assume that the radiation detected with the *ROSAT* from most pulsars is of a nonthermal origin. On the other hand, a correlation between  $L_x$  and  $\dot{E}$  should take place also for radiation emitted by the pulsar PCs because their (thermal) luminosity is also provided by relativistic particles generated in the magnetosphere and accelerated towards the NS surface, so that the PC luminosity should be a fraction of  $\dot{E}$  which goes to heating of the PCs. Moreover, both theoretical (see Section 5.1) and observational estimates of the PC luminosities may happen to be very close to the values predicted by the  $L_x(\dot{E})$  dependence obtained by BT97. For instance, the luminosity of the thermal component in the power-law plus blackbody fit for PSR J0437–4715,  $L_{\text{bol}} = 2.2 \times 10^{30} d_{180}^2 \text{ erg s}^{-1}$  (BT93), is close to the predicted value,  $4 \times 10^{30} \text{ erg s}^{-1}$ . Another example is PSR B1929+10 whose luminosity  $L_{\text{bol}} \simeq 1.2 \times 10^{30} d_{250}^2 \text{ erg s}^{-1}$  inferred from the blackbody fit of both *ROSAT* and *ASCA* data (Yancopoulos et al. 1994; Wang & Halpern 1997) perfectly matches the dependence derived by BT97. In general case, we may expect that the pulsar X-ray radiation contains both thermal (PC) and nonthermal components, both growing with  $\dot{E}$ , and the relation between the thermal and nonthermal fluxes may be different for different objects, depending, in addition to  $\dot{E}$ , on other intrinsic pulsar parameters (e. g., pulsar period  $P$ , magnetic inclination  $\alpha$ ), as well as on the rotational inclination  $\zeta$  (because the radiation beam widths are different for the thermal and nonthermal components). Thus, one cannot rule out that the PC component dominates in some cases, and we explore this possibility for PSR J0437–4715.

An important evidence on the nature of radiation of PSR J0437–4715 could come from deep observations of its high-energy tail, at energies above 1 – 2 keV. Although this object has been detected by *ASCA* (two 20 ks observations) below 3 keV, the results are still not very conclusive because of poor choice of observing modes which did not take into account the presence of a neighboring Seyfert galaxy. Nevertheless, preliminary results show that a spectrum of  $\sim 400$  pulsar photons extracted from the CCD away from the Seyfert galaxy is softer than a power law and resembles more a thermal-like spectrum

(Kawai, Tamura & Saito 1996). This conclusion, however, needs verification based on longer pointed observations in a mode minimizing contamination from the Seyfert.

The conclusion of BT93 and HMM96 that the PSPC spectrum of PSR J0437–4715 cannot be fitted with a single thermal component is based on the assumption that its spectrum coincides with the spectrum of the blackbody radiation. However, spectra emitted by real bodies, including stars, are always different from the Planck spectrum. In particular, if the temperature of a stellar atmosphere grows inward, and the absorption coefficient decreases with frequency (e. g.,  $k_\nu \propto \nu^{-3}$  for the Kramers law), then the spectrum is harder than the blackbody spectrum at high frequencies because we see deeper and hotter layers. This means that if a NS is covered with a fully ionized plasma, whose opacity can be described by the Kramers law, its spectrum is substantially harder at high energies,  $h\nu \gtrsim kT_{\text{eff}}$  (e. g., Pavlov & Shibano 1978). This general property has been demonstrated in models of hydrogen and helium atmospheres of cooling NSs by Romani (1987), Pavlov et al. (1995), Rajagopal & Romani (1996), Zavlin, Pavlov & Shibano (1996; hereafter ZPS96). One can expect that a NS has a purely hydrogen atmosphere if it experienced accretion of the interstellar matter — heavy elements of the accreted matter sink down rapidly due to the strong NS gravitation (Alcock & Illarionov 1980). Since PSR J0437–4715 is a very old object, it is quite plausible that it accreted some matter during its long life, and in this case we may expect that the excess of the observed flux at  $E \gtrsim 0.4 - 0.6 \text{ keV}$  is due to the fact that PSR J0437–4715, including its PCs, is covered by a fully ionized hydrogen atmosphere.

The PC radiation should be inevitably pulsed unless the rotation axis coincides with either the line of sight or the magnetic axis. If it were the blackbody radiation, the shape of the light curves and the pulsed fraction  $f_p$  would remain the same at all photon energies  $E$ . However, the atmosphere radiation has a very important feature — it is anisotropic, with anisotropy (and consequently light curves) depending on energy (Pavlov et al. 1994; Shibano et al. 1995; ZPS96). This dependence is different for different chemical compositions and surface temperatures. E. g., for atmospheres with relatively high temperatures  $\sim 10^6 \text{ K}$  consisting of light elements (hydrogen, helium), the anisotropy increases with increasing  $E$  in the soft X-ray range. This also makes the spectra dependent on the rotation phase. The inter-dependence of the spectral and angular distributions means that the proper interpretation of the observed PC radiation implies fitting of *both the spectra and the light curves with the same PC model*.

The above-described properties of radiation emitted by a PC covered with an atmosphere warrant a new investigation of the soft X-ray radiation observed from PSR J0437–4715, based on the NS atmosphere models. To perform this investigation, we used the *ROSAT* and *EUVE* data analyzed previously by BT93 and HMM96 and com-

bined with the results of new observations carried out with the *ROSAT* High-Resolution Imager (HRI) and *ROSAT* PSPC (Becker et al. 1997). These observations are briefly described in Section 2.

We show that with allowance for the properties of NS atmosphere radiation these joint *ROSAT* and *EUVE* data can be interpreted as thermal radiation of two PCs, *without invoking an additional nonthermal component*. In Section 3 we explore a simplest single-temperature PC model which assumes that both PCs have equal radii  $R_{\text{pc}}$  and uniform temperatures  $T_{\text{pc}}$ , whereas the rest part of the NS surface has a much lower temperature and is invisible in X-rays. Since the magnetic field of PSR J0437–4715 is very low, it cannot affect the radiative properties of the PC atmospheres. Therefore, we use the low-field atmosphere models developed by ZPS96. To calculate the flux as measured by a distant observer, we integrate the specific flux over the visible PC surface with allowance for the gravitational redshift and bending of the photon trajectories. For the case of small PCs ( $R_{\text{pc}} \ll R_{\text{NS}}$ ) with uniform temperatures, a convenient expression for the observable flux is given by Zavlin, Pavlov & Shibano (1995; see their Eq. [A15]). We show that this simple model is generally consistent with the observational data if the PCs are covered with hydrogen or helium, whereas the iron atmosphere model does not fit the spectra (cf. Pavlov et al. 1996b). For the hydrogen and helium models, we estimate  $R_{\text{pc}}$ ,  $T_{\text{pc}}$  and the interstellar hydrogen column density,  $n_H$ .

The fit with the simplest PC model is still not perfect. This is not surprising because it is hard to expect the real PCs to be uniformly heated. On the contrary, due to higher heat conduction of subphotospheric layers, where the energy of accreting relativistic particles is released, the heat can propagate along the surface, eventually heating surface layers out of the “primary” hot spot. This should result in a larger hot region with the temperature decreasing outward. In fact, this mechanism should be more efficient just for low-field pulsars because the strong magnetic fields of ordinary pulsars greatly reduce the transverse conductivity (e. g., Hernquist 1985). To the best of our knowledge, there have been no reliable calculations of the temperature distribution around the pulsar magnetic poles. Thus, to include this effect into consideration, we explore in Section 4 a simple model: the distribution is assumed to be a two-step function (“core+rims”) with two temperatures,  $T_{\text{core}}$  and  $T_{\text{rim}}$ , and two radii,  $R_{\text{core}}$  and  $R_{\text{rim}}$ . We show that this model is fairly consistent, for hydrogen-covered PCs, with all the data available. We discuss the results and implications of our interpretation in Section 5 and draw conclusions in Section 6.

## 2. Observational data and the power-law fit

### 2.1. *ROSAT* PSPC and HRI

We used two data sets obtained during pointed PSPC observations (total  $3172 \pm 58$  counts) and one data set obtained with HRI ( $1517 \pm 39$  counts); the corresponding count rates are  $0.202 \pm 0.004 \text{ s}^{-1}$  and  $0.043 \pm 0.004 \text{ s}^{-1}$ , respectively. Details of these observations are described by BT93 and Becker et al. (1997).

Since no source counts were detected in the PSPC pulse height channels above channel 200, and the PSPC response matrix is not sufficiently known for softest channels, we used channels 10–200 ( $E \approx 0.1 - 2.0 \text{ keV}$ ) for our spectral and temporal analysis. We manually binned the count spectrum into 49 energy bins with the signal-to-noise ratio between 4 and 9 and used this binning for the spectral fitting with the aid of the MIDAS/EXSAS software (Zimmerman et al. 1994).

We used the PSPC and HRI temporal dependences of the source count rate folded with the radio pulsar period by Becker et al. (1997). The PSPC light curves were extracted in 0.1–0.6, 0.6–1.1, 1.1–2.0 and 0.1–2.0 keV energy ranges (13, 9, 9 and 17 phase bins, respectively). The shapes of the light curves from the second data set were compared with those of the first set using a  $\chi^2$  test. The analysis showed that the light curves from both sets of the PSPC data are consistent with each other with a probability  $> 70\%$ , that justifies summation of the light curves from the two PSPC observations.

The combined PSPC light curves show an evidence that the pulsed fraction  $f_p$  depends on energy, in accordance with the dependence reported by BT93 for the first data set. Defining  $f_p$  in the standard way, as the fraction of the total counts lying above the light curve minimum, we obtained an increase from  $f_p = 32 \pm 4\%$  at 0.1–0.6 keV to  $f_p = 44 \pm 8\%$  at 0.6–1.1 keV. Formally, in the 1.1–2.0 keV range the pulsed fraction reaches  $54 \pm 11\%$ , but this value should be considered with caution because of poor statistics ( $\approx 252$  counts in this range). The pulsed fraction in the total energy range is  $f_p = 30 \pm 4\%$ . No phase shifts between the light curves in different energy ranges were found (cf. BT93).

Although the estimated  $f_p$  values indicate that the light curves have different shapes in different energy ranges, they suffer from large uncertainties of the number of counts in the phase bins corresponding to the minima of the observed light curves, being thereby not very reliable estimators. Besides, light curves with equal  $f_p$  can have quite different shapes. Therefore, an independent statistical test is needed to ascertain and quantify statistically the difference of the light curve shapes. The same  $\chi^2$  test shows that the probability that the shapes of the light curves in different ranges are *different* is generally high, between 77% and 92%. Although the difference might be partly due to systematic uncertainties, we believe that the dependence of the light curve shapes and pulsed fractions on energy is statistically reliable (at least, it cannot be

rejected on statistical grounds) and can be considered as an additional argument in favor of thermal origin of the soft X-ray radiation from PSR J0437–4715.

The HRI light curve folded with the radio pulsar period and binned into 11 phase bins results in the pulsed fraction  $f_p = 32 \pm 5\%$ .

## 2.2. EUVE DSI

We used the observational data kindly provided by Jules Halpern and described in detail by HMM96. The total of  $4163 \pm 65$  source counts were collected at the source count rate of  $0.00973 \pm 0.00017 \text{ s}^{-1}$ . This uncertainty ( $\pm 2\%$ ) is due to statistics only; a systematic uncertainty may be as high as 15–20% (Bowyer et al. 1996). The produced light curve with 20 phase bins yields the pulsed fraction  $f_p = 27 \pm 5\%$ .

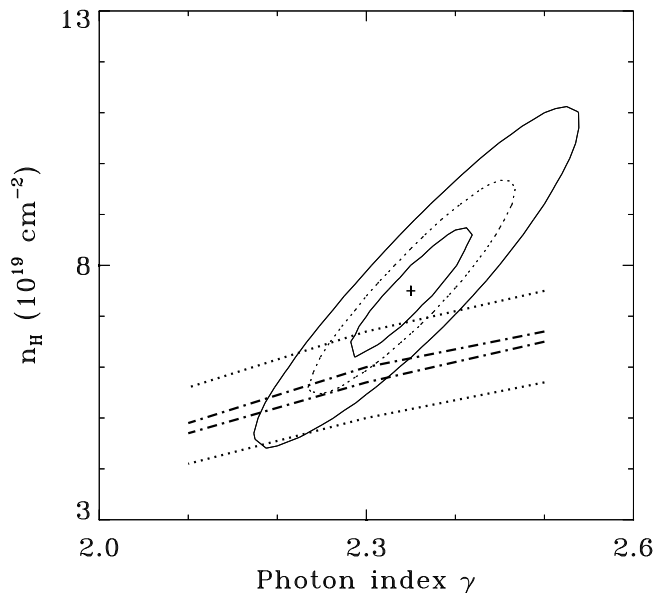


**Fig. 1.** 68%, 90% and 99% confidence contours for the power-law fit to the PSPC spectrum combined from two data sets. Thick dot-dashes are the lines of minimum and maximum DSI fluxes if only statistical errors are taken into account; thick dots correspond to possible  $\pm 15\%$  systematic uncertainty of the DSI effective area.

## 2.3. Power-law fit

A power law with the photon index  $\gamma = 2.35 \pm 0.20$ , intrinsic source luminosity  $L_x = (7.3 \pm 0.8) \times 10^{30} d_{180}^2 \text{ erg s}^{-1}$  in 0.1–2.0 keV and  $n_H = (7.5 \pm 2.3) \times 10^{19} \text{ cm}^{-2}$  provides an acceptable ( $\chi_\nu = 1.08$ ) fit to the combined PSPC spectrum. The parameter values are generally consistent with those obtained by BT93 and HMM96:  $\gamma = 2.6 \pm 0.2$ ,  $n_H = (1.4 \pm 0.5) \times 10^{20} \text{ cm}^{-2}$ ,  $L_x = 9.9 \times 10^{30} d_{180}^2 \text{ erg s}^{-1}$ , and  $\gamma = 2.45 \pm 0.25$ ,  $n_H = (9.2 \pm 4.8) \times 10^{19} \text{ cm}^{-2}$ ,  $L_x = 8.3 \times 10^{30} d_{180}^2 \text{ erg s}^{-1}$ , respectively. The best power-law fit to the combined PSPC spectrum yields the HRI

count rate  $0.044 \text{ s}^{-1}$ , which is compatible with the measured value of  $0.043 \pm 0.004 \text{ s}^{-1}$ .

Folding the same model with the *EUVE* DSI response gives the count rate  $0.00747 \text{ s}^{-1}$ , which is about 20% lower than the observed value. Following HMM96, we tested whether or not the single power-law fits to the PSPC spectrum can be consistent with the DSI flux. We folded each of the trial spectra on a grid of the fitting parameters  $\gamma$  and  $n_H$  through the effective area curve of DSI and obtained a corresponding grid of predicted DSI count rates. Figure 1 presents the 68%, 90% and 99% confidence contours of the PSPC fits in the  $\gamma$ - $n_H$  plane, together with the bands allowed by estimated systematic uncertainties of the DSI response. Figure 1 shows that our joint PSPC+DSI analysis restricts the hydrogen column density to  $n_H = (5.4 - 7.1) \times 10^{19} \text{ cm}^{-2}$ , at a 90% confidence level. This restriction is compatible with that of HMM96,  $n_H = (5 - 8) \times 10^{19} \text{ cm}^{-2}$ , obtained with almost thrice lower number of the PSPC counts. It should be noted, however, that if one adopts the 2% statistical uncertainty for the DSI domain, it does not overlap the 68% PSPC confidence ellipse, so that the joint analysis of the PSPC and DSI data hints that the power-law spectral model may be only *marginally* acceptable. This can be considered as one more reason to test *thermal* models for the soft X-ray radiation of PSR J0437–4715.

## 3. Single-temperature polar cap model

In this Section we analyze the above-described data in terms of the simplest one-component thermal model. We assume that the observed radiation is emitted by two symmetric, uniformly heated PCs around the (dipole) magnetic poles. We consider three chemical compositions for the PC atmospheres, and, for the sake of comparison, the blackbody model for the PC radiation. The fitting parameters for this model are  $n_H$ , the PC (effective) temperature  $T_{pc}$ , and the ratio  $R_{pc}/d$ . The radius  $R_{pc}$  is defined as the distance from the cap edge to the magnetic axis. We fix the distance to the pulsar,  $d = 180 \text{ pc}$  (a most probable value, according to Sandhu et al. 1997), and present the results for  $R_{pc}$  and PC luminosity for this distance. Since the atmosphere spectra and, particularly, light curves depend on the viewing angle, the directions of the magnetic and rotation axes are to be specified. We adopt, for most of our fits,  $\zeta = 40^\circ$  for the angle between the rotation axis and the line of sight, and  $\alpha = 35^\circ$  for the angle between the rotation and magnetic axes (Manchester & Johnston 1995). To specify the gravitational acceleration for calculating the atmosphere models, and the NS mass-to-radius ratio for account of the gravitational bending of the photon trajectories, we adopt  $M_{NS} = 1.4 M_\odot$  and  $R_{NS} = 10 \text{ km}$  for the NS mass and radius. All temperatures and radii here and below are as measured at the pulsar surface.

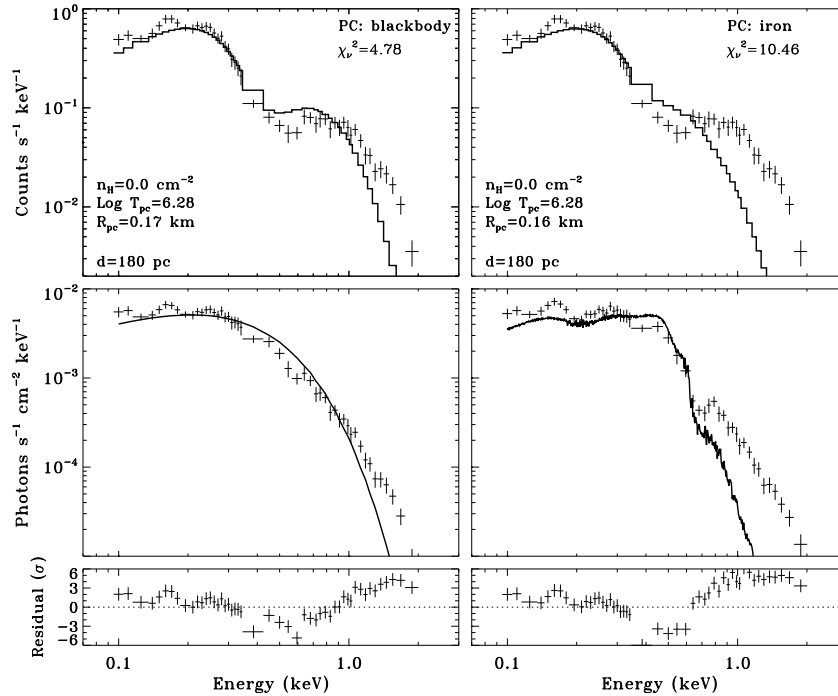


**Fig. 2.** Single PC model fits (blackbody radiation and iron atmosphere) to the PSPC count rate spectrum, with values of best-fit parameters.

### 3.1. PSPC spectral fits

Fitting the combined PSPC spectrum with four models for the PC radiation yields the following results.

*Blackbody.*— In agreement with what was found by BT93 and confirmed later by HMM96 for the first PSPC data set, the single blackbody model fails to fit the combined PSPC spectrum (minimum  $\chi^2_{\nu} = 4.78$ ) because the blackbody spectrum is too soft (steep) at high energies and leaves too large residuals at  $E \gtrsim 0.9$  keV (Fig. 2). Formally, the fit yields  $n_H = (0.0 \pm 1.1) \times 10^{19}$  cm $^{-2}$ ,  $\log T_{pc} = 6.28 \pm 0.03$  and  $R_{pc} = (0.17 \pm 0.02) d_{180}$  km. This gives the bolometric luminosity of two PCs  $L_{bol} = (1.36 \pm 0.25) \times 10^{30} d_{180}^2$  erg s $^{-1}$ .

*Iron atmosphere.*— Because of numerous spectral lines quasi-randomly distributed at  $\sim 0.3 - 3.0$  keV, the smoothed spectra emitted by iron atmospheres in the soft X-ray range are not much different from blackbody spectra at the same temperatures (Rajagopal & Romani 1996; ZPS96). The spectral lines of iron atmosphere spectra cannot be detected by *ROSAT* due to its poor energy resolution. The spectral fit with the iron atmosphere model (right panel of Fig. 2) is even worse than with the blackbody: minimum  $\chi^2_{\nu} = 10.46$ . The lower quality of this fit is caused by the fact (ZPS96) that the iron atmosphere spectra are softer than the blackbody spectra in the soft X-ray range at temperatures  $\sim 10^6$  K.

*Hydrogen atmosphere.*— In comparison with the two cases above, the PC model with hydrogen composition gives a much better fit, with minimum  $\chi^2_{\nu} = 1.68$  (Fig. 3).

Since the hydrogen atmosphere spectra, as well as any other thermal spectra, have an intrinsic decrease towards low energies, they fit the observed spectrum at much lower interstellar hydrogen density,  $n_H = (0.0 \pm 1.7) \times 10^{19}$  cm $^{-2}$ . The other parameters are  $\log T_{pc} = 5.94 \pm 0.03$  and  $R_{pc} = (0.77 \pm 0.13) d_{180}$  km. Since the high-energy tail of the radiation emitted from hydrogen atmospheres is harder than the blackbody tail, the resulting PC temperature is 2.2 times lower than the temperature of the blackbody fit. To provide the same flux,  $R_{pc}$  becomes 4.5 times greater approaching the conventional estimate of  $\sim 1.9$  km. The corresponding bolometric luminosity of two PCs is  $L_{bol} = (1.22 \pm 0.22) \times 10^{30} d_{180}^2$  erg s $^{-1}$ , comparable with that for the blackbody model. We checked that the fitting parameters are very stable with respect to the choice of energy channels (binning) of the PSPC count rate spectrum — only the minimum value of  $\chi^2_{\nu}$  varies slightly. For example, the fit in 20-140 channels (0.2 – 1.4 keV range) with 19 bins yields the same values of  $n_H$ ,  $T_{pc}$  and  $R_{pc}$ , with minimum  $\chi^2_{\nu} = 1.16$ .

*Helium atmosphere.*— For helium-covered PCs (right panel of Fig. 3), the quality of the fit and the values of the model parameters are similar to those for the hydrogen composition. A smaller value of the minimum  $\chi^2_{\nu} = 1.37$  is due to the fact that at  $T \sim 10^6$  K the spectrum of the helium atmosphere is slightly harder than that of the hydrogen atmosphere (ZPS96). Generally, the fits with hydrogen and helium models are almost indiscernible.

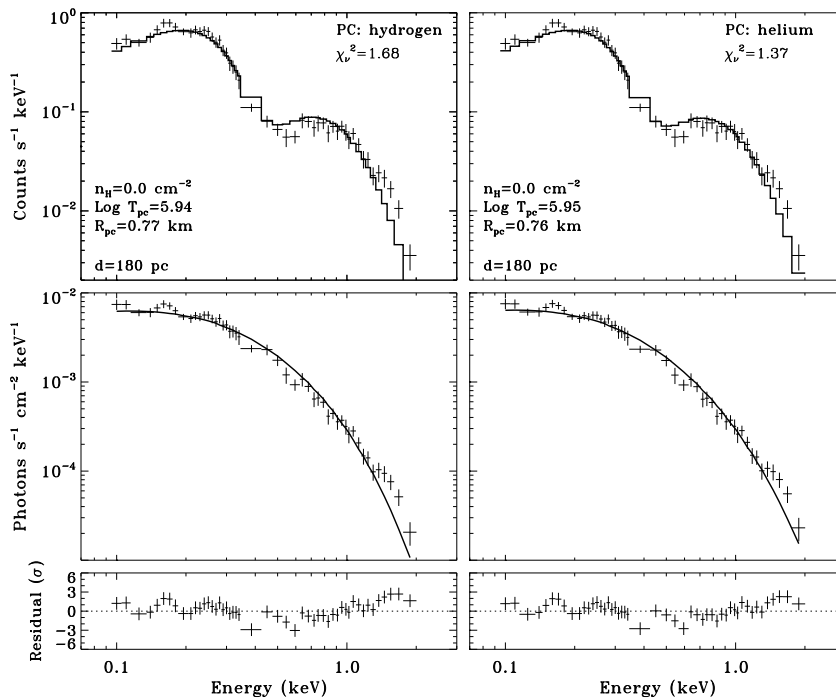


**Fig. 3.** The same as in Fig. 2 for the hydrogen and helium atmospheres.

Although the hydrogen and helium PC models fit the PSC spectrum much better than the blackbody model, there still is an excess of the observed radiation at  $E \gtrsim 1.5$  keV (see Fig. 3). The excess can be partly due to systematic errors of the high-energy PSC response which may be as high as 20%. Irrespective of that, the excess can be naturally explained by simplicity of the single-temperature PC model — if there is a smaller area of a greater temperature within the PC, it can easily provide the excess high-energy quanta, the possibility we explore in Section 4. The single-temperature approximation, however, enables us to show that the spectrum can be fitted with a purely thermal model provided that the PCs are covered by a hydrogen or helium atmosphere, whereas the hypothesis about the iron surface of the PCs can be firmly rejected. (A similar conclusion has been drawn by Rajagopal & Romani (1996) who, however, obtained substantially different PC parameters because they fitted the observed spectrum without allowance for the limb-darkening and light bending.) We do not expect that other heavy-element compositions of the NS surface could fit the observed spectrum — they should also lead to emitted spectra much softer than the spectra of hydrogen or helium atmospheres. We consider the hydrogen atmosphere more natural than the helium one (e. g., if the atmosphere was formed due to accretion of the hydrogen-rich interstellar matter or matter from the binary companion), and we explore consistency of this hypothesis with the HRI and DSI results, as well as with the light curves observed with the three instruments.

### 3.2. Analysis of the ROSAT HRI and EUVE DSI count rates

Figure 4 shows the confidence contours for the parameters of the hydrogen PC fit to the PSC spectrum. We checked that any point from the 99% PSC confidence region produces the model HRI count rate within the observed range. The best parameters of the PSC spectral fit give a too high count rate for the EUVE DSI,  $0.01136 \text{ s}^{-1}$ , which does not even get into the  $\pm 15\%$  systematic uncertainty range around the observed value. The reason is that the formal best fit yields  $n_H = 0$  (no interstellar absorption), which clearly is not a realistic value. However,  $n_H$  is determined with some uncertainties, and even a small value of  $n_H$  can noticeably decrease the DSI flux and make the DSI and PSC count rates consistent with each other. Similar to the case of the power-law model (Section 2), we computed the bands in the parameter planes allowed by the observed DSI flux. The thick dot-dash lines in Fig. 4 correspond to the DSI count rates of  $0.00973 \pm 0.00017 \text{ cnts/s}$ . The shaded regions show the domains of the model parameters allowed by all the three instruments at the 68% confidence level. If we adopt the  $\pm 15\%$  uncertainty for the observed DSI count rate (thick dots), the allowed regions become much broader.

Thus, there exist a domain of the model parameters compatible with all of the detected count rates and with the PSC spectra:  $n_H = (0.5 - 0.9) \times 10^{19} \text{ cm}^{-2}$ ,  $\log T_{pc} = 5.92 - 5.95$  and  $R_{pc} = (0.75 - 0.85) d_{180} \text{ km}$ . The corresponding area and bolometric luminosity of two PCs are  $A = (3.5 - 4.5) d_{180}^2 \text{ km}^2$  and  $L_{bol} = (1.2 -$

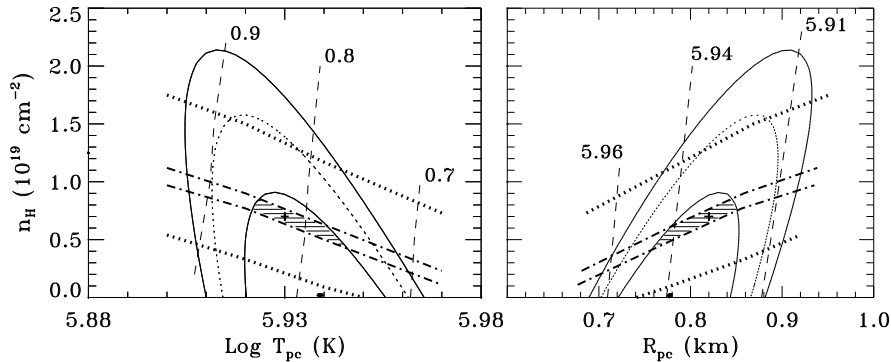


**Fig. 4.** Projections of the 68, 90 and 99% confidence domains onto two parameter plains for the hydrogen PC fit to the PSPC spectrum. Thin dashes correspond to constant values (numbers near the lines) of third parameter. Filled squares show the best-PSPC-fit parameters (cf. Fig. 3). Thick dot-dashes and dots are the lines of constant DSI fluxes (cf. Fig. 1). The shaded regions give the model parameters allowed by the count rates of all the three instruments. Crosses correspond to the “best PC model”.

$1.3) \times 10^{30} d_{180}^2 \text{ erg s}^{-1}$ . Similar to the case of the power-law fit, the main role of the *EUVE* data is that these data enable us to restrict the  $n_H$  value; the difference is that for the thermal PC model the range of jointly acceptable  $n_H$  values lies above the best-PSPC-fit value, and they are an order of magnitude lower than for the joint power-law fit. This implies a higher ionized fraction, and a lower mean number density of the interstellar hydrogen in the direction to PSR J0437–4715 (see Discussion). The center of the allowed three-dimensional parameter domain is given, approximately, by the following values:  $n_H = 0.7 \times 10^{19} \text{ cm}^{-2}$ ,  $\log T_{\text{pc}} = 5.93$  and  $R_{\text{pc}} = 0.82 d_{180} \text{ km}$ , which can be considered as a best joint PSPS+HRI+DSI fit (marked with crosses in Fig. 4). For the sake of brevity, we call this set of parameters “the best PC model” for the rest of this Section.

### 3.3. Light curve analysis

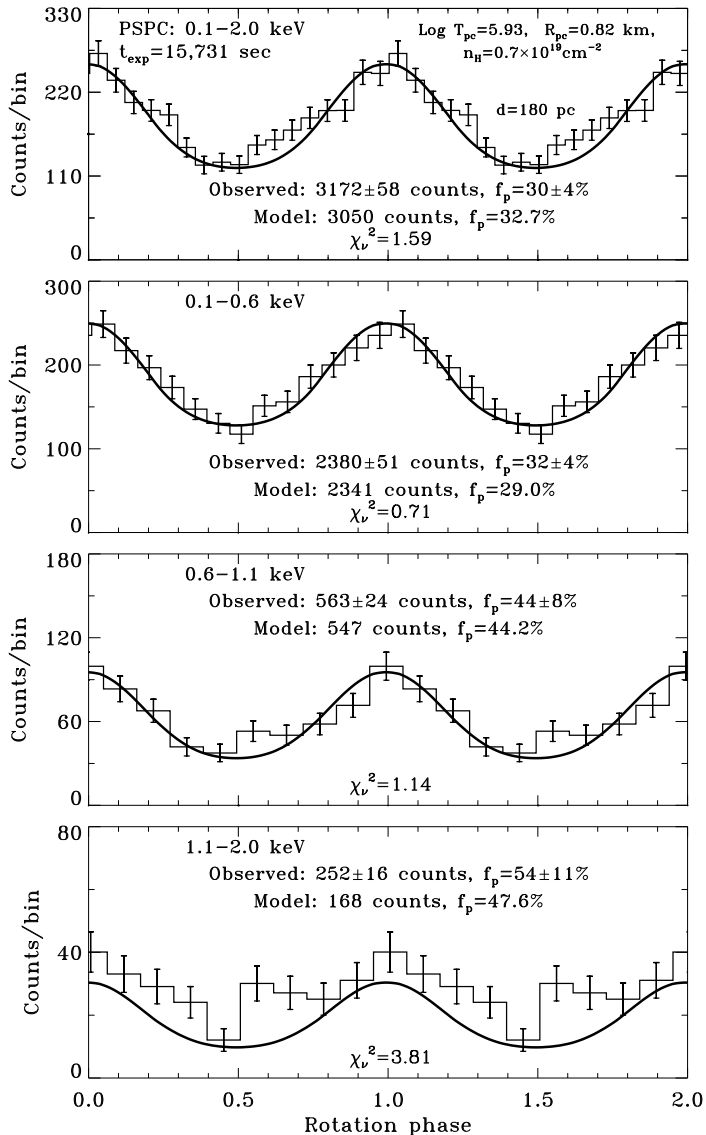
Now we should test whether the PC model obtained from the analysis of the PSPC spectrum and HRI and DSI count rates fits the light curves detected with these instruments. To do that, we computed the spectra for 80 rotation phases,  $0 \leq \phi \leq 1$ , for the best PC model and convolved the spectra at each phase with the PSPC, HRI and DSI responses. Then, we binned these model count rates into the phase bins adopted for the observed light curves to compare the light curves with the aid of the  $\chi^2$ -test. The  $\chi^2$  value depends on how we co-align the phases for the model and the observed light curves. Since the reference phases of the observed light curves were chosen arbitrarily, we may vary the phase shift between the model and observed light curves to minimize  $\chi^2$ . (Of course, the shifts in different energy ranges should not differ from each other by more than a fraction of the bin width; ideally, the difference should be comparable with, or less than, the instrument time resolution).

Figure 5 presents the adjusted model and observed PSPC light curves for the four energy ranges. We define the zero rotation phase as the phase when the angle  $\theta$  between the magnetic axis and the line of sight equals its minimum value,  $\theta_{\text{min}} = \zeta - \alpha = 5^\circ$ ; this phase corresponds to the maximum of the model light curve, whereas the minimum lies at  $\phi = 0.5$ , corresponding to  $\theta = \theta_{\text{max}} = \zeta + \alpha = 75^\circ$ . The difference of the phase shifts applied to minimize  $\chi^2$  does not exceed  $1/80$  of the rotational period, which corresponds to  $0.07 \text{ ms}$ , about one half of the the *ROSAT* time resolution. As is seen in Fig. 5, the best PC model yields the light curves in excellent agreement with those observed in the  $0.1 - 0.6$  and  $0.6 - 1.1 \text{ keV}$  ranges — not only the pulsed fractions are within the statistical uncertainties, but also the  $\chi_\nu^2$  values are small enough. For the  $1.1 - 2.0 \text{ keV}$  range, the model  $f_p$  is within the observed uncertainty, but the fit is formally unacceptable ( $\chi_\nu^2 = 3.81$ ). This is not surprising in view of the aforementioned deficit of PC counts with respect to observed in this energy range.

Figure 6 shows the observed *ROSAT* HRI and *EUVE* DSI light curves. It is worth noting that the difference between the phase shift applied to adjust the observed PSPC and HRI light curves to the model ones is as small as  $1/80$ . The coincidence of the model and observed light curves is fairly good for both HRI and DSI.

The results above were obtained for  $\zeta = 40^\circ$ ,  $\alpha = 35^\circ$ , and the standard NS mass and radius. The angles, however, are not very certain as this pulsar shows a complicated variation of linear polarization angle across the eight-component mean radio pulse (Manchester & Johnston 1995). In principle, the interpretation of the soft X-ray data adopted in the present paper can reduce this uncertainty — one can fit the data with the PC model considering  $\alpha$  and  $\zeta$  as fitting parameters. These angles, as well as the (unknown) ratio  $M_{\text{NS}}/R_{\text{NS}}$ , affect insignificantly the spectral fit parameters ( $n_H$ ,  $T_{\text{pc}}$  and  $R_{\text{pc}}$ ). However,





**Fig. 5.** Observed and model PSPC light curves in four energy ranges. The model curves correspond to the “best PC model” (model parameters in the upper panel).

the shape of the light curves and  $f_p$  are very sensitive to the choice of  $\alpha$ ,  $\zeta$  and  $M_{\text{NS}}/R_{\text{NS}}$ . For example, an alternative set of the angles,  $\zeta = 24^\circ$  and  $\alpha = 20^\circ$ , obtained with another treatment of polarization data (Gil & Krawczyk 1997), results, for  $M_{\text{NS}}/R_{\text{NS}} = 0.14 M_\odot/\text{km}$ , in a too low pulsed fraction,  $f_p = 15.3\%$  in the whole PSPC energy range, so that the PC model is in clear disagreement with observations ( $\chi_\nu^2 = 3.52$ ) — see Fig. 7. To provide an acceptable fit at this set of angles, the pulsar mass is to be very low,  $M_{\text{NS}} < 0.5 M_\odot$  at any  $R_{\text{NS}}$  allowed by the equations of state of NS interiors (Pavlov et al. 1997). One more example shown in Fig. 7 demonstrates the importance of the gravitational bending of photon trajectories: if this effect is neglected, the best PC model yields a light curve with strong pulsations,  $f_p = 76.8\%$ , resulting in a

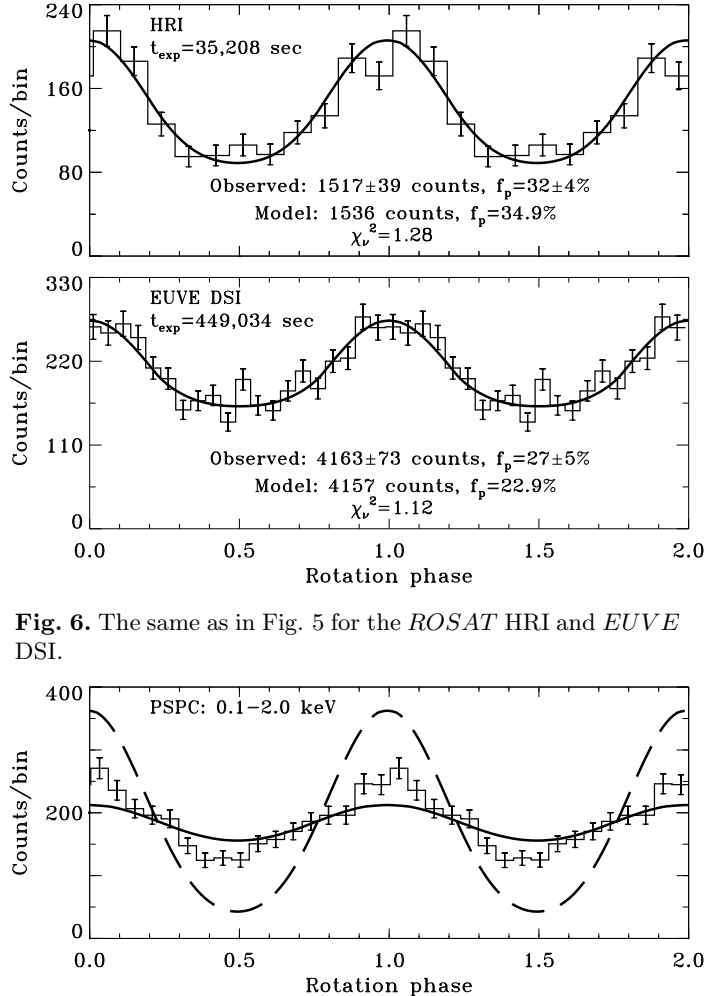


**Fig. 6.** The same as in Fig. 5 for the *ROSAT* HRI and *EUVE* DSI.

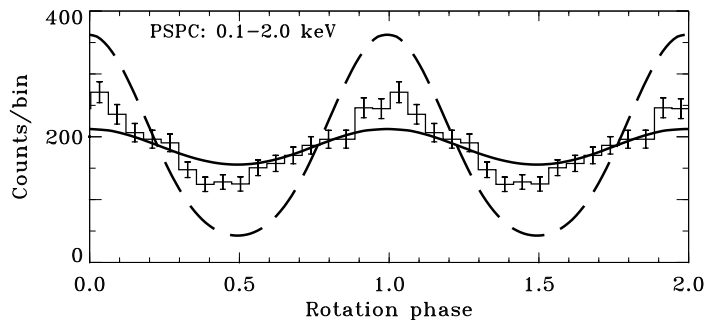


**Fig. 7.** Two examples of hydrogen PC light curves: for another set of the angles ( $\zeta = 24^\circ$  and  $\alpha = 20^\circ$ ; solid) and for the best PC model without allowance for the gravitational bending (dashes).

great deviation,  $\chi_\nu^2 = 29.1$ . The mass-to-radius ratio can be also considered as a fitting parameter to provide better coincidence of the light curves and put constraints on the equation of state of the NS interiors.

#### 4. Two-temperature polar cap model

Motivated by the results of Section 3, we examine a more complicated PC model which allows, in the first approximation, for a non-uniform temperature distribution along the PC surface. We adopt a two-step approximation, “core+rim”, with  $T_{\text{core}} > T_{\text{rim}}$  and  $R_{\text{core}} < R_{\text{rim}}$ . The definitions of  $R_{\text{core}}$  and  $R_{\text{rim}}$  are analogous to  $R_{\text{pc}}$  in Section 3. This model contains, together with  $n_H$ , five fitting parameters. It is natural to expect that  $T_{\text{rim}} < T_{\text{pc}} < T_{\text{core}}$  and  $R_{\text{core}} < R_{\text{pc}} < R_{\text{rim}}$ , where  $T_{\text{pc}}$  and  $R_{\text{pc}}$  are the parameters of the one-component PC model, so that the rim and the core should be responsible for the soft and hard spectral components of this two-component model. We re-

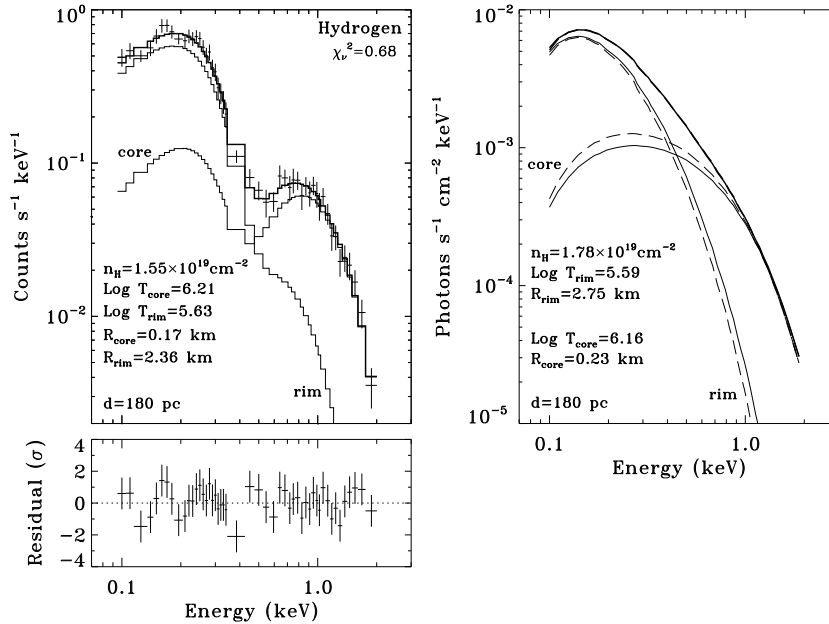


**Fig. 8.** Two-component (“core+rim”) fit to the PSPC spectrum with five free parameters (best values in the upper-left panel). Photon spectral fluxes are shown in the right panel for the five-parameter fit (solid curves) and for the fit with fixed values of  $T_{\text{core}}$  and  $R_{\text{core}}$  (dashes).

tain the same assumptions on the pulsar angles, mass, radius and distance as earlier.

#### 4.1. Iron atmosphere

As one could expect for a two-component model, the iron atmosphere model yields an acceptable fit of the PSPC spectrum (minimum  $\chi^2_{\nu} = 0.72$ ,  $\nu = 44$ ), with the best-fit parameters  $n_H = 7.92 \times 10^{19} \text{ cm}^{-2}$ ,  $\log T_{\text{core}} = 6.57$ ,  $\log T_{\text{rim}} = 5.67$ ,  $R_{\text{core}} = 0.04 d_{180} \text{ km}$  and  $R_{\text{rim}} = 8.36 d_{180} \text{ km}$ . However, the value of  $R_{\text{rim}}$  is very close to the adopted pulsar radius  $R_{\text{NS}} = 10 \text{ km}$ . This means that the soft component is emitted from almost the *whole* NS surface with the uniform temperature  $T_{\text{rim}}$ . By virtue of this, *the rim cannot produce the pulsed fraction  $f_p \simeq 30\%$  observed in the 0.1–0.6 keV range (the model  $f_p$  does not exceed a few percent)*. Since the light curves cannot be fitted with the same model as the spectra, we conclude that the hypothesis about the iron NS surface is incompatible with the thermal model for the soft X-ray radiation of PSR J0437–4715. Thus, we exclude the iron atmosphere model from further consideration, as well as the two-component blackbody model which also leads to  $R_{\text{rim}} \simeq R_{\text{NS}}$ .

#### 4.2. Hydrogen atmosphere

The model count rate spectra in Fig. 8 correspond to the best spectral fit with the following parameters:  $n_H = 1.55 \times 10^{19} \text{ cm}^{-2}$ ,  $\log T_{\text{core}} = 6.21$ ,  $\log T_{\text{rim}} = 5.63$ ,  $R_{\text{core}} = 0.17 d_{180} \text{ km}$  and  $R_{\text{rim}} = 2.36 d_{180} \text{ km}$  (minimum  $\chi^2_{\nu} = 0.68$ ,  $\nu = 44$ ). The corresponding bolometric luminosity of

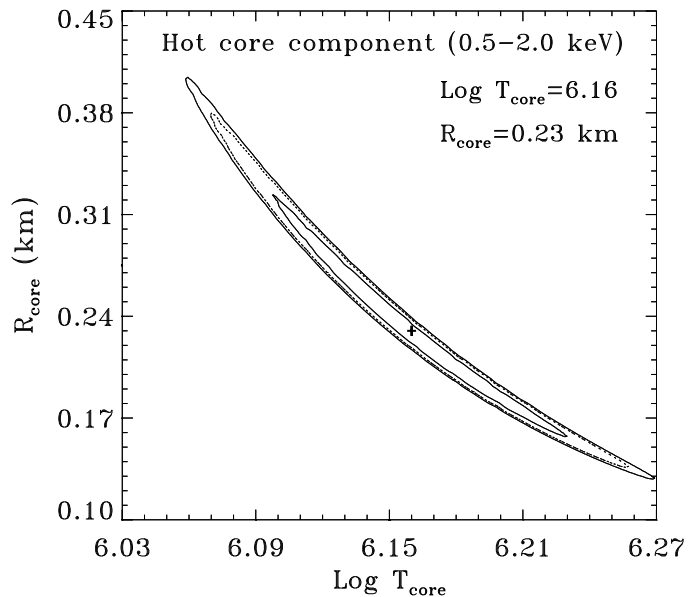


**Fig. 9.** Confidence contours for the parameters of hard (core) component in the two-component PSPC spectral fit.

two rims and cores,  $L_{\text{bol}} = 1.37 \times 10^{30} d_{180}^2 \text{ erg s}^{-1}$  (51% and 49% from the cores and rims, respectively), is close to that of the single-temperature PC model.

However, in spite of quite realistic values of these parameters, they are very uncertain, which follows from large formal errors provided by the fitting code. Although these errors, calculated from the derivatives of the fit statistics, are not reliable, they indicate that the parameters are strongly correlated, and the best fit gives only qualitative

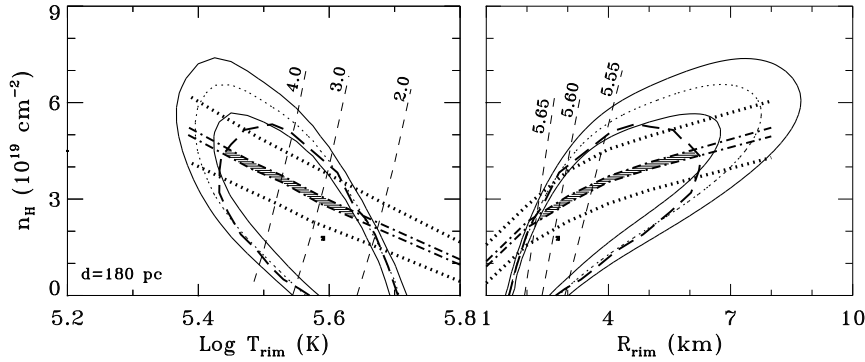


**Fig. 10.** Projections of 68, 90 and 99% confidence domains for the three-parameter PSPC spectral fit of the soft (rim) component (thin solid and dot lines), with fixed best core parameters (cf. Fig. 9). Thick dashed lines show restriction (68% confidence level) obtained from the light curves in the whole PSPC energy range. Other notations are the same as in Fig. 4.

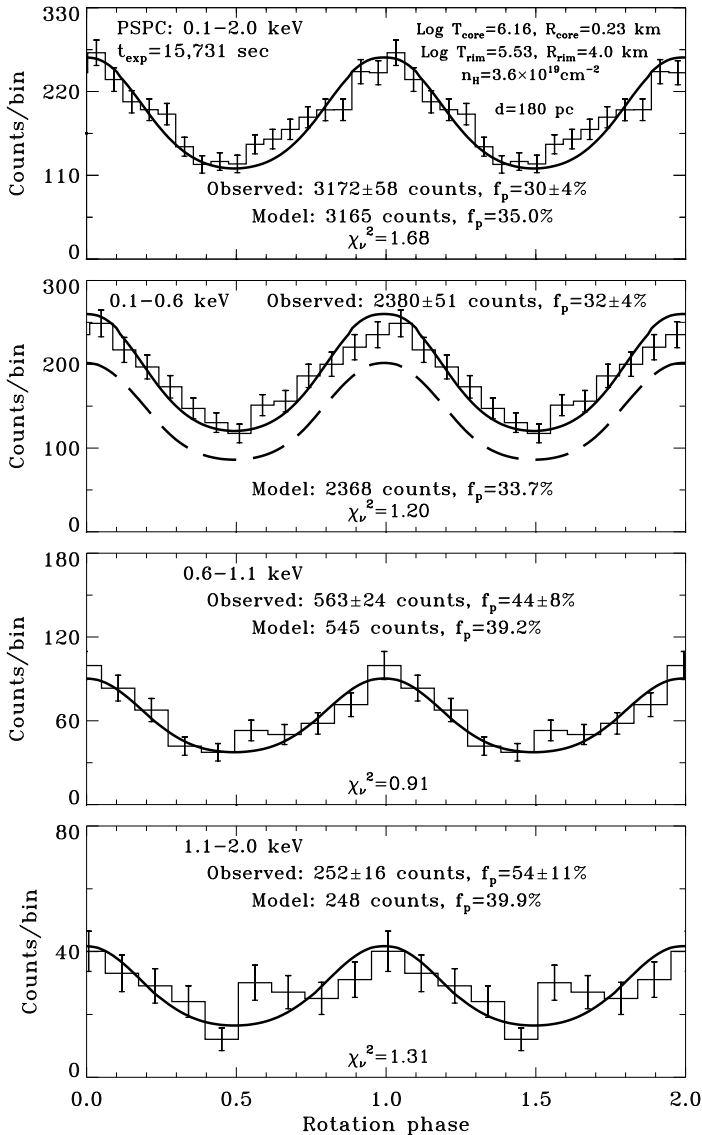


**Fig. 11.** The same as in Fig. 5 for the “core+rim” two-component fit. The dashes show the contribution to the 0.1–0.6 keV light curve from the rim component

estimates of the parameter values. In principle, the parameter ranges can be reduced with the use of the *ROSAT* HRI and *EUVE* DSI data, but it would require an extremely time-consuming analysis of five-dimensional confidence volumes. A practical way to solve the problem is prompted by the shapes of the best-fit component spectra — we see that the hot core component gives the main contribution at higher energies, above 0.4–0.6 keV, whereas the rims are responsible for the flux at lower energies. Therefore, we can first fit the hard channels separately with a single-temperature cap model (notice that  $n_H$  of expected magnitudes does not affect spectra at these energies), and then fix some set(s) of  $T_{\text{core}}$  and  $R_{\text{core}}$  and fit the rim component with the three fitting parameters,  $n_H$ ,  $T_{\text{rim}}$  and  $R_{\text{rim}}$ .

The first step with 21 energy bins in the 53–200 channels gives the best-fit parameters of the hot core,  $\log T_{\text{core}} = 6.16 \pm 0.07$  and  $R_{\text{core}} = (0.23 \pm 0.09) d_{180} \text{ km}$  ( $\chi^2_{\nu} = 0.92$ ,  $\nu = 19$ ), in accordance with the two-component results. Figure 9 demonstrates the confidence contours for this fit.

At the second step, we fixed the best pair of  $T_{\text{core}}$  and  $R_{\text{core}}$  obtained at the first step and fitted the total PSPC count rate spectrum with the “core+rim” model (the best-fit parameters are given in the right panel of Fig. 8). We see that the separate fitting of the hard and soft (core and rim) components yields spectra fairly close to those obtained with the five-parameter fit.

The projections of the three-dimensional confidence regions for the parameters of the soft component are shown in Fig. 10. The regions are still too broad, in spite of the reduced number of the fitting parameters, because the parameters are strongly correlated (e. g.,  $n_H \propto \ln R_{\text{rim}}$  at a given  $T_{\text{rim}}$ ) due to narrowness of the soft-energy range. In particular, the 99% confidence surface allows the outer rim radius to be comparable with  $R_{\text{NS}}$  at lower  $T_{\text{rim}}$  and higher  $n_H$ . However, large values of  $R_{\text{rim}}$  are not consistent with the strong time modulation of the observed flux at low energies, and upper limits for  $R_{\text{rim}}$  and  $n_H$  (and a lower limit

on  $T_{\text{rim}}$ ) are to be obtained from the light curve analysis. Since the values of  $R_{\text{rim}}$  involved in the light curve fitting are relatively large, we have to integrate over the rim surface making use of the exact equations for the gravitational bending (Zavlin et al. 1995), instead of previously used approximate approach for  $R_{\text{rim}} \ll R_{\text{NS}}$ . Fitting the PSPC light curve in the whole energy range with the two-component model restricts the radius:  $R_{\text{rim}} < 6.2, 6.7$  and  $7.1$  km; temperature:  $\log T_{\text{rim}} > 5.45, 5.42$  and  $5.39$ ; and hydrogen column density:  $n_H/(10^{19} \text{ cm}^{-2}) < 4.4, 4.8$  and  $5.2$ ; at 68%, 90% and 99% confidence levels, respectively. The projections of the 68% confidence region are shown in Fig. 10.

Further constraints on the fitting parameters follow from the comparison with the *EUVE* DSI count rate (HRI count rate is consistent with the PSPC fits and does not provide additional restrictions of the fitting parameters). The DSI count rate corresponding to the best PSPC fit (with the hard and soft components fitted separately) is  $0.01196 \text{ s}^{-1}$ , i. e., 23% higher than the observed value. We used the same approach as for the single-temperature PC model and found the three-dimensional volumes in the parameter space compatible with the measured DSI count rates with the 2% (statistical) and 15% (systematic) uncertainties (thick dash-dot and dot curves in Fig. 10). The shaded areas in Fig. 10 delimit projections of the parameter volume compatible with the data collected with all the three instruments at the 68% confidence level (neglecting poorly-known systematic uncertainties). We chose a point with  $n_H = 3.6 \times 10^{19} \text{ cm}^{-3}$ ,  $\log T_{\text{rim}} = 5.53$  and  $R_{\text{rim}} = 4.0 d_{180} \text{ km}$  (“best core+rim model”). The bolometric luminosity for this model is  $L_{\text{bol}} = 1.57 \times 10^{30} d_{180}^2 \text{ erg s}^{-1}$ .

Following the approach used for the one-component PC model, we plotted the two-component light curves corresponding to this model (Figs. 11 and 12). The comparison shows a satisfactory agreement with the observed light curves. We see that the pulsations at lower energies are stronger for the “core+rim” model than for the single-temperature PC model ( $f_p = 33.7\%$  vs.  $29.0\%$  for the  $0.1\text{--}0.6 \text{ keV}$  PSPC range, and  $25.7\%$  vs.  $22.9\%$  for DSI). This is due to the fact that the rim, which mainly contributes at  $E \lesssim 0.5 \text{ keV}$  (Fig. 8), has a lower temperature,  $T_{\text{rim}} < T_{\text{pc}}$ , resulting in higher anisotropy of the emergent radiation (ZPS96). The rim emits 74% of all the PSPC counts with  $f_p = 37.1\%$  at  $E = 0.1 - 0.6 \text{ keV}$ , and 87% of counts with  $f_p = 31.6\%$  in the DS range. The soft component gives less than a half of the total HRI counts, and we obtain almost the same light curve fits for the single-temperature PC and “core+rim” models (cf. Figs. 6 and 12). In the whole PSPC range there is a bigger share of the total radiation with  $f_p = 36.4\%$  coming from the rim, that leads to higher pulsations in the summed light curve than for the simplest PC model ( $f_p = 35.0\%$  vs.  $32.7\%$ , respectively).

Finally, we can conclude that the two-component hydrogen “core+rim” model satisfactorily matches to the

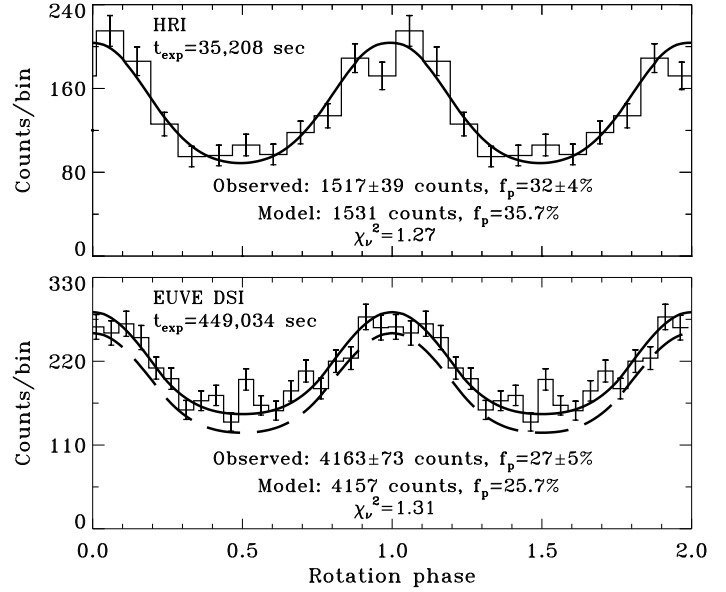


**Fig. 12.** The same as in Fig. 11 for the *ROSAT* HRI and *EUVE* DSI, with separate contribution from the rim component (dashes).

spectral data and the light curves provided by all the three instruments.

### 4.3. Helium atmosphere

As expected, this model yields virtually the same results as the hydrogen atmosphere model. For instance, the best five-parameter fit gives  $n_H = 1.98 \times 10^{19} \text{ cm}^{-2}$ ,  $\log T_{\text{core}} = 6.14$ ,  $\log T_{\text{rim}} = 5.57$ ,  $R_{\text{core}} = 0.26 d_{180} \text{ km}$ , and  $R_{\text{rim}} = 2.94 d_{180} \text{ km}$ , with  $\chi^2_\nu = 0.70$ . Since, in addition, the hydrogen composition looks more natural, the helium atmosphere model does not require a detailed separate analysis.

## 5. Discussion

### 5.1. Comparison with predictions of radio pulsar models

It is interesting to compare the inferred PC properties with those predicted by different radio pulsar models. The *slot-gap model* (Arons & Scharlemann 1979; Arons 1981) predicts the following energy flux of relativistic particles incident on the stellar surface (Arons 1981)

$$F \simeq 1 \times 10^{19} \left( \frac{\mu_{26}}{3.4} \right) \left( \frac{5.75 \text{ ms}}{P} \right)^{19/8} \left( \frac{4}{f_\rho} \right)^{1/4} \left( \frac{10 \text{ km}}{R_{\text{NS}}} \right)^{9/8} \left( \frac{\sin \alpha}{\sin 35^\circ} \right)^{5/4} \text{ erg cm}^{-2} \text{ s}^{-1}, \quad (1)$$

where  $\mu_{26}$  is the magnetic moment in units of  $10^{26} \text{ G cm}^3$ ,  $f_\rho$  is the ratio of the dipole radius of curvature to the actual radius of curvature,  $1 \lesssim f_\rho \lesssim 7$  for the parameters of PSR J0437–4715. The model is applicable for  $P <$

$3.1R_{10}^{-3/17}f_\rho^{10/17}$  ms; this corresponds to  $f_\rho > 2.85R_{10}^{0.3}$  for  $P = 5.75$  ms, and we adopt an intermediate value  $f_\rho = 4$  for estimates. If most of this energy is reradiated, the effective temperature and luminosity are

$$T_{\text{eff}} = 6.5 \times 10^5 \left(\frac{\mu_{26}}{3.4}\right)^{1/4} \left(\frac{5.75 \text{ ms}}{P}\right)^{19/32} \left(\frac{4}{f_\rho}\right)^{1/16} \left(\frac{10 \text{ km}}{R_{\text{NS}}}\right)^{9/32} \left(\frac{\sin \alpha}{\sin 35^\circ}\right)^{5/16} \text{ K}, \quad (2)$$

$$L_{\text{cap}} = 0.6 \times 10^{30} \left(\frac{f_a}{0.5}\right) \left(\frac{\mu_{26}}{3.4}\right) \left(\frac{5.75 \text{ ms}}{P}\right)^{27/8} \left(\frac{4}{f_\rho}\right)^{1/4} \left(\frac{R_{\text{NS}}}{10 \text{ km}}\right)^{15/8} \left(\frac{\sin \alpha}{\sin 35^\circ}\right)^{5/4} \text{ erg s}^{-1}, \quad (3)$$

where  $f_a$  is the ratio of the polar cap area to its canonical value,  $11.4R_{10}^3(5.75 \text{ ms}/P) \text{ km}^2$  ( $f_a \simeq 0.5$  for the original slot-gap model which implies that the particle acceleration zone is associated with “favorably curved” open field lines). We see that the predicted temperature is 20–30% lower than the temperature  $T_{\text{pc}}$  inferred from the single-temperature PC model, but it is higher than  $T_{\text{rim}}$ . The predicted luminosity is in excellent agreement, for  $f_\rho = 4$  and  $f_a = 0.5$ , with the observed value. Since the observed luminosity is almost independent of the PC temperature distribution ( $2L = (1.0 - 1.5) \times 10^{30} \text{ erg s}^{-1}$  for both the single-temperature and two-temperature PC models), it is the most suitable parameter to compare with, and we should conclude that the slot-gap model agrees very well with the suggested interpretation of the soft X-ray radiation from PSR J0437–4715.

According to the *outer-gap model* (e. g., Cheng, Ho & Ruderman 1986), PSR J0437–4715 is near the pulsar “death line”,  $P_{\text{death}} = 5.8(B/3.4 \times 10^8 \text{ G})^{5/12} \text{ ms}$ , that implies high efficiency of the gamma-ray radiation produced by primary  $e^\pm$  accelerated in vacuum gaps in the outer magnetosphere of the pulsar. The total (maximum) flux of relativistic  $e^+$  (or  $e^-$ ) impinging on the PC from the starward end of the acceleration zone can be estimated as

$$\dot{N} \sim \frac{\mu\Omega^2}{2ec} = 1.4 \times 10^{31} \left(\frac{\mu_{26}}{3.4}\right) \left(\frac{5.75 \text{ ms}}{P}\right)^2 \text{ s}^{-1}, \quad (4)$$

and the luminosity is  $L_{\text{cap}} = \dot{N}\gamma_f m_e c^2$ , where  $\gamma_f$  is the Lorentz factor of particles when they reach the NS surface. While traveling to the surface, the particles lose a fraction of their initial energy  $\gamma_i m_e c^2$  via curvature radiation, so that (cf. Halpern & Ruderman 1993; HMM96)

$$\gamma_f = \left[ \frac{1}{\gamma_i^3} + \frac{2e^2\Omega}{m_e c^3} \ln \left( \frac{r_{\text{min}}}{R_{\text{NS}}} \right) \right]^{-1/3} = \left[ \frac{1}{\gamma_i^3} + \left( \frac{1}{3.65 \times 10^6} \right)^3 \left( \frac{5.65 \text{ ms}}{P} \right) \ln \left( \frac{r_{\text{min}}}{R_{\text{NS}}} \right) \right]^{-1/3}, \quad (5)$$

where  $r_{\text{min}}$  is the minimum distance of the accelerator from the NS center. Adopting  $r_{\text{min}} \simeq (1/3)r_{\text{lc}} \simeq 90(P/5.75 \text{ ms}) \text{ km}$ , the first term in the square brackets can be neglected if  $\gamma_i \gg 3 \times 10^6$  (the latter value is much lower than  $\gamma_{\text{max}} \sim 10^7 - 10^8$  limited by the curvature radiation losses). In this case,  $\gamma_f \simeq 2.8 \times 10^6$ , and the expected PC luminosity,  $L_{\text{cap}} \sim 3.2 \times 10^{31} \text{ erg s}^{-1}$ , exceeds the observed value by a factor of 40–60. The model PC luminosity would agree with the observed one only if we assume  $\gamma_i \simeq \gamma_f \simeq 6 \times 10^4 \sim 10^{-3}\gamma_{\text{max}}$ . Thus, we should conclude that either the  $e^\pm$  energies at the starward accelerator end are much lower than those expected from the curvature radiation losses, or there exists a mechanism reducing the particle flux  $\dot{N}$  which may reach the NS surface. In particular, the estimate (5) assumes the relativistic particles impinge onto the canonical PC area  $A = (\pi\Omega R^3/c) \simeq 11 \text{ km}^2$ . If the actual area is 40–60 times smaller (a “primary” cap radius is 250–300 m, compatible with our  $R_{\text{core}}$ ), then, at the same (Goldreich–Julian) current density, the estimated luminosity coincides with that observed. An evidence of the reduced efficiency of the particle accelerator is provided by the upper limit on the luminosity of gamma-rays above 100 MeV,  $L_\gamma < 1.7 \times 10^{32} = 0.04\dot{E}$  (Fierro et al. 1995). Since the same particle accelerator is responsible for PC heating, HMM96 suggest that an upper limit for the luminosity of one PC can be evaluated as 0.04 times the above-estimated maximum value,  $L_{\text{cap}} < 1.3 \times 10^{30} \text{ erg s}^{-1}$ , very comfortable with the observed range of  $(0.6 - 0.8) \times 10^{30} \text{ erg s}^{-1}$ .

In the *model of Beskin, Gurevich and Istomin* (1993), the energy of relativistic particles impinging onto the PCs per unit time is

$$\dot{E}_{\text{surf}} \simeq \frac{Q^2}{1+K} \dot{E}, \quad (6)$$

where  $Q = 0.52(P/5.75 \text{ ms})^{11/10}(\dot{P}/1.99 \times 10^{-20})^{-2/5}$  and  $K$  is a multiplication coefficient, the number of particles which are knocked out from the NS surface by an impacting relativistic particle. The temperature of the polar cap is estimated as

$$T_{\text{eff}} = \frac{3.8 \times 10^6}{(1+K)^{1/4}} \left( \frac{P}{5.75 \text{ ms}} \frac{\dot{P}}{1.99 \times 10^{-20}} \right)^{1/20} \text{ K}. \quad (7)$$

This temperature is consistent with the observed values,  $\sim 1 \times 10^6$ , only for large multiplication coefficient,  $K \simeq 200$ , much greater than the maximum values,  $K_{\text{max}} \simeq 1$  and  $\simeq 20$  calculated by Bogovalov & Kotov (1989) for  $\gamma_f = 2 \times 10^6$  and  $10^7$ , plausible Lorentz factors for PSR J0437–4715. Moreover, the same calculations show that  $K$  sharply decreases with decreasing  $B$  from  $\simeq 10^{12} \text{ G}$  and becomes  $\ll 1$  at  $B \lesssim 2 \times 10^{11} \text{ G}$ . Thus, we have to conclude that either this model strongly overestimates the PC temperature and luminosity, or the multiplication coefficient is much greater than calculated.

### 5.2. Implications for the magnetic field geometry and the NS mass and radius

The fits of the spectra and of the light curves presented in this paper were obtained for fixed values of the angles  $\zeta = 40^\circ$  and  $\alpha = 35^\circ$  inferred by Manchester & Johnston (1995) from the phase dependence of the position angle of the radio polarization. Since these angles were determined approximately, and it is not trivial to estimate their uncertainties from the radio data, we cannot exclude that their true values may be different. We also adopted canonical values for the NS mass and radius,  $M_{\text{NS}} = 1.4M_\odot$  and  $R_{\text{NS}} = 10$  km, whereas the true mass and radius may differ from these values. We have demonstrated (see Fig. 7) that the shape of the light curves is very sensitive to the values of  $\zeta$ ,  $\alpha$  and  $M_{\text{NS}}/R_{\text{NS}}$ . This opens a new opportunity to constrain these quantities using them as free parameters for the light curve fitting. This analysis is presented elsewhere (Pavlov et al. 1997). Here we only mention that for *any* allowed values of  $\alpha$  and  $\zeta$ , the mass-to-radius ratio is constrained as  $M_{\text{NS}} < 1.7M_\odot (R_{\text{NS}}/10 \text{ km})$ , whereas for  $\alpha = 35^\circ$ ,  $\zeta = 40^\circ$  we obtained  $1.4 < (M_{\text{NS}}/M_\odot)/(R_{\text{NS}}/10 \text{ km}) < 1.6$ . The latter inequality means that if the NS mass equals  $1.4M_\odot$ , its radius is  $8.8 < R_{\text{NS}} < 10.0$  km.

### 5.3. Implications for the interstellar hydrogen

We have shown that interpretation of the soft X-ray data in terms of thermal-like radiation from PCs yields systematically lower values for the intervening hydrogen column density than the power-law fits of the spectrum. For instance, BT93 found  $n_H = (1.4 \pm 0.5) \times 10^{20} \text{ cm}^{-2}$  for the one-component power-law fit, whereas we obtained  $n_H \lesssim 2 \times 10^{19} \text{ cm}^{-2}$  and  $n_H = (1-5) \times 10^{19} \text{ cm}^{-2}$  for the single- and two-temperature PC models, respectively. It is useful to compare these values with those inferred from observations of other objects close towards PSR J0437–4715 ( $l = 253^\circ$ ,  $b = -42^\circ$ ;  $d = 180$  pc). The pulsar is in the southern third galactic quadrant ( $180^\circ < l < 270^\circ$ ,  $b < 0^\circ$ ), apparently within the famous low HI column region that extends out to 200–300 pc at  $210^\circ \lesssim l \lesssim 265^\circ$  (at least for  $b \gtrsim -30^\circ$  — see, e. g., Paresce 1984; Welsh 1991). For instance, two stars of close longitudes and distances,  $\epsilon$  CMa ( $l = 240^\circ$ ,  $b = -11^\circ$ ,  $d = 187$  pc) and  $\beta$  CMa ( $l = 226^\circ$ ,  $b = -14^\circ$ ,  $d = 220$  pc), show the neutral hydrogen densities as low as  $\log n_{\text{HI}} = 18.0-18.5$  and  $18.2-18.4$ , respectively (Fruscione et al. 1994; Welsh 1991). The densities in directions of two other stars within the low density region, RE 0503–289 ( $l = 231^\circ$ ,  $b = -35^\circ$ ,  $d = 90$  pc) and RE 0457–281 ( $l = 229^\circ$ ,  $b = -36^\circ$ ,  $d = 90$  pc), with latitudes closer to that of the pulsar (farther from the Galactic plane), albeit with twice smaller distances, are even lower:  $\log n_{\text{HI}} = 17.3-17.8$  and  $17.1-17.9$ . A white dwarf WD 0320–540 ( $l = 267^\circ$ ,  $b = -52^\circ$ ,  $d = 103$  pc), which is likely near the boundary of the low-density region, shows

$\log n_{\text{HI}} = 18.9-19.2$ . Based on these values and observations of other (scarce) stars in this region of the sky (Fruscione et al. 1994, Welsh 1991; and references therein), we expect that plausible neutral hydrogen column for PSR J0437–4715 should not exceed  $n_{\text{HI}} \simeq (1-3) \times 10^{19} \text{ cm}^{-2}$ .

Interstellar absorption of X-rays enters the spectral fits through the attenuation function,  $\exp(-n_H\sigma)$ , where  $\sigma$  is the effective cross section per hydrogen atom calculated under the assumption that the interstellar hydrogen is not ionized (e. g., Morrison & McCammon 1983). The effective hydrogen column density  $n_H$  coincides, naturally, with  $n_{\text{HI}}$  for the nonionized ISM, but for the partially ionized hydrogen we have  $n_{\text{HI}} < n_H < n_H^{\text{tot}}$ , where  $n_H^{\text{tot}} \simeq n_{\text{HI}} + n_e$  is the total (neutral plus ionized) hydrogen column density. With the electron column density  $n_e = 0.81 \times 10^{19} \text{ cm}^{-2}$ , known from the pulsar dispersion measure, we can restrict the mean ionization degree of hydrogen,  $\xi = n_e/n_H^{\text{tot}}$ , as  $n_e/(n_e + n_H) < \xi < n_e/n_H$ . If we adopt  $n_H = (1-3) \times 10^{19} \text{ cm}^{-2}$  as a plausible estimate, the ionization degree  $0.2 < \xi < 0.8$  is noticeably greater, and the (total) mean number density in the direction towards PSR J0437–4715,  $n_H^{\text{tot}}/d = (0.02-0.07)d_{180}^{-1} \text{ cm}^{-3}$ , is lower than the estimates,  $\xi \simeq 0.04-0.1$  and  $n_H^{\text{tot}}/d \simeq (0.16-0.34)d_{180}^{-1} \text{ cm}^{-3}$ , obtained from the power-law fit. The inferred high ionization is in line with  $\xi \approx 0.9$  found by Gry, York & Vidal-Madjar (1985) in the direction to  $\beta$  CMa. It is worth noting that the mean number density inferred from our PC model fits is fairly close to the ISM density of the ambient medium around the pulsar estimated by equating the ram pressure of the interstellar medium to the pulsar wind pressure at the apex of the pulsar wind’s bow shock (see, e. g., HMM96):  $n_H^{\text{tot}} = \dot{E}/(4\pi r_w^2 v_p^2 c m_H) \simeq 0.08 \text{ cm}^{-3}$ , where the distance from the pulsar to the apex of the bow shock,  $r_w = 2.4 \times 10^{16} \text{ cm}$ , and the velocity of the pulsar,  $v_p = 118 \text{ km s}^{-1}$ , are evaluated for  $d = 180$  pc.

### 5.4. X-rays from other millisecond pulsars: thermal or nonthermal?

The fact that all available X-ray and EUV data are consistent with our interpretation still does not prove that this interpretation is unique — it often happens that the same data can be equally well fitted with quite different models. Therefore, it is important to verify that the hypothesis does not contradict to observations of similar objects. According to BT97, soft X-ray radiation has been observed from seven millisecond pulsars. At least one of them, PSR B1821–24 ( $P = 3.05$  ms,  $\dot{E} = 2.2 \times 10^{36} \text{ erg s}^{-1}$ ), shows a strong evidence that its radiation is of a nonthermal (magnetospheric) origin — its spectrum, observed with *ASCA* up to 10 keV, can be fitted with a power law, and its X-ray pulses are sharp (Saito et al. 1997). Thus, if we assume that PCs is a phenomenon common for all millisecond pulsars, we must explain why this phenomenon is not observed for PSR B1821–24. This can be done with the use of the aforementioned pulsar models. If the correct

estimate obtained for the PC luminosity from the slot-gap model is not a chance coincidence, we may expect that the luminosity is scaled as  $L_{\text{cap}} \propto \dot{P}^{1/2} P^{-23/8}$ , and the bolometric luminosity from two PCs of PSR B1821–24 can be estimated as  $L_{\text{bol}} \sim (6 - 9) \times 10^{31} \text{ erg s}^{-1}$ . This estimate is much lower than the luminosity  $L_x = 1.7 \times 10^{33} \text{ erg s}^{-1}$  inferred by Saito et al. (1997). If we adopt the outer-gap model and assume that the accelerator efficiency is reduced by the same factor for all pulsars, then the luminosity is scaled as  $L_{\text{cap}} \propto \dot{P}^{1/2} P^{-11/6}$ , which yields  $L_{\text{bol}} \sim (3 - 5) \times 10^{31} \text{ erg s}^{-1}$  for PSR B1821–24, even less than for the slot-gap model. Moreover, even the maximum possible PC luminosity predicted by the outer-gap model remains lower than observed. Thus, it is not surprising that the PC radiation is not seen from this pulsar, being overwhelmed by a nonthermal soft X-ray radiation. Saito et al. (1997) speculate that the high luminosity of the non-thermal radiation may be associated with large values of the magnetic field at the light cylinder,  $B_{\text{lc}} \sim 1.5 \times 10^6 \text{ G}$ , close to that of the Crab pulsar and much higher than  $B_{\text{lc}} \sim 1.7 \times 10^4 \text{ G}$  for PSR J0437–4715.

The nature of X-ray radiation from other five millisecond pulsars is much less certain because of small numbers of counts detected. Their luminosities in the *ROSAT* range, inferred under the assumption of a power-law spectrum with the photon index  $\gamma = 2$ , obey the same dependence,  $L_x \simeq 0.001\dot{E}$ , as ordinary pulsars (BT97), and they are greater than the PC luminosities predicted for these objects by the slot-gap model (scaled to PSR J0437–4715). However, the ratios of the observed to predicted luminosities, ranging from  $\simeq 1.6$  for PSR J1012+5307 to  $\simeq 10$  for PSR J0751+1907, are smaller than  $\simeq 25$  for PSR B1821–24. Since the power-law model always yields a higher luminosity than the PC model (because of higher  $n_H$  needed to suppress the intrinsically high low-energy flux), one may expect that the luminosities inferred from the PC interpretation would be compatible with those predicted by equation (3). In addition, as Arons (1981) emphasizes, equation (3) gives a *minimum* expected luminosity — although the luminosity of PSR J0437–4715 coincides with that minimum, PC luminosities of other pulsars may be greater. Thus, the soft X-ray radiation of at least some other millisecond pulsars can be partly supplied by their PCs, although a nonthermal component may also be present and may even dominate. To resolve the dilemma, and to separate the two components, further observations are needed. At present, we can only say that both possibilities should be explored, and complementary interpretations are still viable for some pulsars.

## 6. Summary and conclusions

We have shown that both the spectra and the light curves of the soft X-ray radiation of PSR J0437–4715 observed with the *ROSAT* PSPC and HRI and *EUVE* DSI can be interpreted as *thermal radiation from two hydrogen-*

*covered polar caps*. The simplest, single-temperature PC model allows us to estimate typical PC radius,  $R_{\text{pc}} \sim 1 \text{ km}$ , and temperature,  $T_{\text{pc}} \sim 1 \times 10^6 \text{ K}$ . The successful fitting of the data with the two-temperature model indicates that the PC temperature may be non-uniform, decreasing from  $T_{\text{core}} \sim (1.1 - 1.8) \times 10^6 \text{ K}$  at a PC core with a typical size  $R_{\text{core}} \sim 150 - 400 \text{ m}$  down to  $T_{\text{rim}} \sim (3 - 5) \times 10^5 \text{ K}$  at a much greater radius  $R_{\text{rim}} \sim 2 - 6 \text{ km}$ , so that the heated area may comprise a considerable fraction of the NS surface. The bolometric luminosity of the two PCs is  $L_{\text{bol}} = (1.0 - 1.6) \times 10^{30} d_{180}^2 \text{ erg s}^{-1}$ , that is  $\sim (2 - 4) \times 10^{-4}$  of the total energy loss of the pulsar is absorbed and re-emitted by the PCs.

We emphasize that the proposed interpretation is based essentially upon the *neutron star atmosphere models* — the data cannot be interpreted as purely thermal PC radiation with the simplistic blackbody model. Moreover, with the aid of the NS atmosphere models we show that the emitting layers should be depleted of heavy elements, which can be naturally explained by the plausible assumption that the old NS has experienced accretion of the hydrogen-rich matter during its long life-time.

The successful fits of the *EUVE* and *ROSAT* light curves in different energy ranges with the PC models are possible only if the energy-dependent limb-darkening of the hydrogen atmospheres is taken into account. The shape of the light curves is also very sensitive to the bending of photon trajectories in the strong gravitational field of the NS and to the orientations of the rotational and magnetic axes of the pulsar. We obtained the satisfactory fits assuming  $M_{\text{NS}} = 1.4M_{\odot}$  and  $R_{\text{NS}} = 10 \text{ km}$ , with the magnetic inclination angle,  $\alpha = 35^\circ$ , and viewing angle,  $\zeta = 40^\circ$ , inferred from radio observations. We have demonstrated that the effect of the gravitational bending on the light curves can provide important information on the NS mass-to-radius ratio.

The hydrogen column density towards the PSR J0437–4715,  $n_H \sim (1 - 3) \times 10^{19} \text{ cm}^{-2}$ , as well as strong ionization of hydrogen,  $\xi > 20\%$ , estimated from the PC model fits are consistent with the ISM properties obtained from observations of other objects in the vicinity of the pulsar, whereas the power-law fit yields greater  $n_H$  and lower  $\xi$ . This can be considered as one more argument in favor of thermal origin of the X-ray radiation of PSR J0437–4715.

The inferred PC temperature, radius and, especially, luminosity are in excellent agreement with the predictions of the slot-gap pulsar model (Arons 1981). The upper limit on the PC luminosity provided by the outer-gap pulsar model (Cheng et al. 1986) exceeds the observed value. This model becomes compatible with our results if a reduced efficiency of the particle accelerator, consistent with the upper limit on the gamma-ray flux from the pulsar, is assumed.

Radio pulsar models predict that heated PCs is a common phenomenon inherent to all active pulsars. By virtue of this, the dependence  $L_x \simeq 0.001\dot{E}$  found by BT97 for 26

pulsars detected with the *ROSAT* determines a fraction of the rotational energy loss re-emitted in X-rays *by both nonthermal and thermal processes*. Contributions of these two mechanisms to the total X-ray flux depend on various factors, such as pulsar period, radius, magnetic field, etc. In some pulsars (e. g., PSR B1821–24) the thermal-like soft X-ray radiation from PCs may happen to be less intensive than the nonthermal radiation generated in the pulsar magnetosphere. For instance, both the slot-gap and outer-gap models predict the luminosity of PCs of PSR B1821–24 much lower than the luminosity observed with the *ROSAT* and *ASCA*.

Although all the available observations of PSR J0437–4715 are consistent with the suggested PC interpretation, and this interpretation is supported by the theoretical pulsar models and by indirect arguments, we still cannot completely exclude that the same data, collected in the relatively narrow energy range, could be interpreted with another model — for instance, as a combination of the PC radiation and magnetospheric radiation. Hence, the proposed interpretation can be considered as complementary to the nonthermal interpretation discussed by BT97. A crucial test would be provided by observations of this object at energies  $\gtrsim 1 - 2$  keV, which would enable one to firmly discriminate between the power-law and thermal-like spectra, or to separate their contributions. Such observations could be carried out by *ASCA* (with a sufficiently long exposure) and by the forthcoming *AXAF*, *XMM* and *ASTRO-E* missions. Important data could be also obtained from observations of the pulsar in the UV range ( $1200 \lesssim \lambda \lesssim 3000$  Å) with the *HST*. In particular, such observations would enable one to measure the temperature of the entire NS surface (cf. Pavlov, Stringfellow & Córdoba 1996a) and to elucidate other possible heating mechanisms competing with the PC heating.

For more accurate and reliable interpretation of the future observations, more theoretical work is highly desirable. In particular, the temperature distribution over the NS surface within and around the PCs should be investigated (and further used to fit the data), and the nonthermal X-ray spectrum and beam shape should be calculated.

*Acknowledgements.* We are grateful to Werner Becker and Jules Halpern for providing us with the *ROSAT* PSPC/HRI and *EUVE* DSI observational data prior to publication. We are greatly indebted to Joachim Trümper and Werner Becker for their collaboration and fruitful, stimulating discussions. V. E. Zavlin acknowledges the Max-Planck fellowship. G. G. Pavlov is thankful to the Max-Planck-Institut für Extraterrestrische Physik for the warm hospitality. This work was partially supported through the INTAS grant 94-3834, DFG-RBRF grant 96-02-00177G and NASA grant NAG5-2807.

## References

Alcock C., Illarionov A. F., 1980, *ApJ*, 235, 534  
 Arons J., 1981, *ApJ*, 248, 1099  
 Arons J., Scharlemann, E. T., 1979, *ApJ*, 231, 854.

Bailyn C. D., 1993, *ApJ*, 411, L83  
 Becker W., Trümper J. (BT93), 1993, *Nat.*, 365, 528  
 Becker W., Trümper J. (BT97), 1997, *A&A* (accepted)  
 Becker W., Trümper J., Brazier K. T. S., Belloni T., 1993, *IAU Circular* 5701  
 Becker W., et al., 1997 (in preparation)  
 Bell J. F., Bailes M., Bessell M. S., 1993, *Nature*, 364, 603  
 Bell J. F., Bailes M., Manchester R. N., Weisberg J. M., Lyne A. G., 1995, *ApJ*, 440, L81  
 Beskin V. S., Gurevich A. F., Istomin Ya. N., 1993, *Physics of Pulsar Magnetosphere*. Cambridge Univ. Press, Cambridge  
 Bogovalov S. V., Kotov, Yu. D. 1989, *Sov. Astron. Lett.*, 15, 185  
 Bowyer S., et al., 1996, *ApJS*, 102, 129  
 Cheng A. F., Ruderman M. A., 1980, *ApJ*, 235, 576  
 Cheng K. S., Ho C., Ruderman M. A., 1986, *ApJ*, 300, 500  
 Danziger I. J., Baade D., Della Valle M., 1993, *ApJ*, 408, 179  
 Edelstein J., Foster R. S., Bowyer S., 1995, *ApJ*, 454, 442  
 Fierro J. M., et al., 1995, *ApJ*, 447, 807  
 Fruscione A., Hawkins I., Jelinsky P., Wiercigroch A., 1994, *ApJS*, 94, 127  
 Gil J., Krawczyk A., 1997, *MNRAS*, 285, 561  
 Gry C., York D. G., Vidal-Madjar A., 1985, *ApJ*, 296, 593  
 Greiveldinger C., et al., 1996, *ApJ*, 465, L35  
 Halpern J. P., Ruderman M., 1993, *ApJ*, 415, 286  
 Halpern J. P., Martin C., Marshall H. L. (HMM96), 1996, *ApJ*, 462, 908  
 Hernquist L., 1985, *MNRAS*, 213, 313  
 Johnston S., et al., 1993, *Nature*, 361, 613  
 Kawai N., Tamura K., Saito Y., 1996, in: Burke W. R. (ed). *ESA's Report to the 31st COSPAR Meeting (ESA-SP 1194)*. Noordwijk, ESA (in press)  
 Manchester R. N., Johnston S., 1995, *ApJ*, 441, L65  
 Manning R. A., Willmore A. P., 1994, *MNRAS*, 266, 635  
 Michel F. C., 1991, *Theory of Neutron Star Magnetospheres*. Univ. of Chicago Press, Chicago  
 Morrison R., McCammon D., 1983, *ApJ*, 270, 119  
 Ögelman H., 1995, in: Alpar M. A., Kiziloğlu Ü., van Paradijs J. (eds). *The Lives of the Neutron Stars*. Kluwer, Dordrecht, p. 101  
 Paresce F., 1984, *AJ*, 89, 1022  
 Pavlov G. G., Shibanov Yu. A., 1978, *Sov. Astron.*, 22, 214  
 Pavlov G. G., Shibanov Yu. A., Ventura J., Zavlin V. E., 1994, *A&A*, 289, 837  
 Pavlov G. G., Shibanov Yu. A., Zavlin V. E., Meyer R. D., 1995, in: Alpar M. A., Kiziloğlu Ü., van Paradijs J. (eds). *The Lives of the Neutron Stars*. Kluwer, Dordrecht, p. 71  
 Pavlov G. G., Stringfellow G. S., Córdoba F. A., 1996a, *ApJ*, 467, 370  
 Pavlov G. G., Zavlin V. E., Becker W., Trümper J., 1996b, *BAAS*, 28, 947  
 Pavlov G. G., Zavlin V. E., Trümper J., 1997, in: Olinto A., Frieman J., Schramm D. (eds). *18th Texas Symposium on Relativistic Astrophysics*. World Scientific Press (in press)  
 Radhakrishnan V., Cooke D. J., 1969, *Astrophys. Lett.*, 3, 225  
 Rajagopal M., Romani R. W., 1996, *ApJ*, 461, 327  
 Romani R. W., 1987, *ApJ*, 313, 718  
 Romani R. W., 1996, *ApJ*, 470, 469  
 Saito Y., et al., 1997, *ApJ*, 477, L37  
 Sandhu J. S., et al., 1997, *ApJ*, 478, L95  
 Seward F. D., Wang Z.-R., 1988, *ApJ*, 332, 193



- Shibanov Yu. A., Zavlin V. E., Pavlov G. G., Ventura J., 1995,  
in: Alpar M. A., Kiziloğlu Ü., van Paradijs J. (eds). The  
Lives of the Neutron Stars. Kluwer, Dordrecht, p. 91
- Sturner S. J., Dermer C. D., Michel F. C., 1995, ApJ, 445, 736
- Wang F. Y.-H., Halpern J. P., 1997, ApJ, 482, 159
- Welsh B. Y., 1991, ApJ, 373, 556
- Yancopoulos S., Hamilton T. T., Helfand D., 1994, ApJ, 429,  
832
- Zavlin V. E., Shibanov Yu. A., Pavlov G. G., 1995, Astron.  
Let., 21, 149
- Zavlin V. E., Pavlov G. G., Shibanov Yu. A. (ZPS96), 1996,  
A&A, 315, 141
- Zimmermann H.-U., et al., 1994, EXSAS Users's Guide. MPE  
Report 257, ROSAT Scientific Data Center, Garching